# Enhanced Spontaneous Emission at Third-Order Dirac Exceptional Points in Inverse-Designed Photonic Crystals

Zin Lin,[1,*] Adi Pick,[2,3] Marko Lončar,[1] and Alejandro W. Rodriguez[4]
[1]John A. Paulson School of Engineering and Applied Sciences, Harvard University, Cambridge, Massachusetts 02138, USA
[2]Department of Physics, Harvard University, Cambridge, Massachusetts 02138, USA
[3]Department of Mathematics, Massachusetts Institute of Technology, Cambridge, Massachusetts 02139, USA
[4]Department of Electrical Engineering, Princeton University, Princeton, New Jersey 08544, USA
(Received 19 May 2016; published 30 August 2016)

We formulate and exploit a computational inverse-design method based on topology optimization to demonstrate photonic crystal structures supporting complex spectral degeneracies. In particular, we discover photonic crystals exhibiting third-order Dirac points formed by the *accidental* degeneracy of monopolar, dipolar, and quadrupolar modes. We show that, under suitable conditions, these modes can coalesce and form a third-order exceptional point, leading to strong modifications in the spontaneous emission (SE) of emitters, related to the local density of states. We find that SE can be enhanced by a factor of 8 in passive structures, with larger enhancements $\sim\sqrt{n^3}$ possible at exceptional points of higher order $n$.

DOI: 10.1103/PhysRevLett.117.107402

Dirac cones in photonic systems have received much attention because of their connections to intriguing optical properties, enabling large-area photonic-crystal (PhC) surface-emitting lasers [1], *Zitterbewegung* of photons [2], appearance of zero-index behavior [3,4], and as precursors to nontrivial topological effects [5–7]. Recent work also showed that Dirac-point degeneracies can give rise to rings of exceptional points [8]. An exceptional point (EP) is a singularity in a non-Hermitian system where two or more eigenvectors and their corresponding complex eigenvalues coalesce, leading to a nondiagonalizable, defective Hamiltonian [9,10]. EPs have been studied in various physical contexts, most notably lasers and atomic as well as molecular systems [11,12]. In recent decades, interest in EPs has been reignited in connection with non-Hermitian parity-time symmetric systems [13], especially optical media involving carefully designed gain and loss profiles [14–20], where they can lead to intriguing phenomena such as excess noise [21,22], chiral modes [23], directional transport [24,25], and anomalous lasing behavior [26–28]. Also recently, it became possible to directly observe EPs in photonic crystals (PhCs) [8] and optoelectronic microcavities [29]. Thus far, however, the main focus of these works has been the effect of second-order exceptional points (EP2s) realized through photonic radiations, where only two modes coalesce; apart from a few mathematical analyses [30–32] or works focused on acoustic systems [33], there has been little or no investigation into the design and consequences of EPs of higher order (where more than two modes collapse).

In this Letter, we formulate and exploit a powerful inverse-design method, based on topology optimization (TO), to develop complex photonic crystals supporting Dirac points formed out of the *accidental* degeneracy [34] of modes belonging to different symmetry representations. We show that such higher-order Dirac points can be exploited to create third-order exceptional points (EP3s) along with complex contours of EP2s. Furthermore, we consider possible enhancements and spectral modifications in the spontaneous emission (SE) rate of emitters, showing that the local density of states (LDOS) at an EP3 (14) can be enhanced eightfold (in passive systems) and can exhibit a cubic Lorentzian spectrum under special conditions. More generally, we find enhancement factors $\sim\sqrt{n^3}$ with increasing EP order $n$. Although the area of photonic inverse design is not new [35–37], only recently has it gained traction, with most works [37–41] primarily focused on improving the performance of conventional devices with known functionalities. Here, we show that these methods can be extended and leveraged to realize structures exhibiting unusual spectral properties.

Dirac cones are traditionally identified in simple geometries involving cylindrical pillars or holes on a square or triangular lattice [3,42]. They arise from modal degeneracies induced by underlying lattice symmetries (e.g., $C_{4v}$ or $C_{3v}$) and through fine-tuning of a few geometric parameters [3,43]. Recently, it was demonstrated [8] that a Dirac cone at the $\Gamma$ point of a PhC with $C_{4v}$ symmetry can give rise to a ring of EP2s. Such a feature is formed by degenerate monopolar ($M$) and dipolar ($D$) modes, which transform according to $A$ and $E$ representations of the $C_{4v}$ group [3,43]. Even though the degeneracy consists of one monopole and two dipoles, the induced EP is of the second order, with only the monopole and one of the dipoles colliding, while the coalescence of the dipole partner is prevented by symmetry [8]. Below, we show that an EP3 can be induced by a completely "accidental" third-order degeneracy (D3) at the $\Gamma$ of an inverse-designed PhC

 

lacking $C_{4v}$ symmetry, involving modes of monopolar ($M$), dipolar ($D$), and quadrupolar ($Q$) nature.

*Coupled-mode analysis.*—The band structure in the vicinity of such a D3 can be modeled by an approximate Hamiltonian of the form [42]:

$$\mathcal{H} = \begin{pmatrix} \omega_0 & v_{MD}k_x & 0 \\ v_{MD}k_x & \omega_0 & v_{QD}k_y \\ 0 & v_{QD}k_y & \omega_0 \end{pmatrix} \tag{1}$$

Here, $\omega_0$ is the triply degenerate angular frequency and $\mathbf{k} = (k_x, k_y)$ is the in-plane Bloch wave vector while $v_{ij}, i, j \in \{M, D, Q\}$ characterizes the mode mixing away from the $\Gamma$ point, to first order in $\mathbf{k}$ [42]. Note that the diagonalization of this Hamiltonian yields a completely real band structure comprising a Dirac cone and a flat band, $\omega = \omega_0, \omega_0 \pm \sqrt{v_{MD}^2 k_x^2 + v_{QD}^2 k_y^2}$.

To induce an EP, non-Hermiticity can be introduced by the addition of a small imaginary perturbation to the Hamiltonian,

$$\mathcal{H} = \begin{pmatrix} \omega_0 + i\gamma_M & v_{MD}k_x & 0 \\ v_{MD}k_x & \omega_0 + i\gamma_D & v_{QD}k_y \\ 0 & v_{QD}k_y & \omega_0 + i\gamma_Q \end{pmatrix}, \tag{2}$$

with $\gamma > 0$ ($< 0$) representing a small amount of absorption (amplification) or radiation. An EP3 is associated with a third-order algebraic multiplicity in the roots of the characteristic polynomial $P(\omega)$ of $\mathcal{H}$ and thus can be enforced by vanishing derivatives up to second order,

$$\det(\mathcal{H} - \omega\mathbb{I}) = P(\omega) = 0, \tag{3}$$

$$P'(\omega) = 0, \tag{4}$$

$$P''(\omega) = 0. \tag{5}$$

Solving the above equations for $\omega, k_x$, and $k_y$ yields the EP3:

$$\omega^{\mathrm{EP3}} = \omega_0 + \frac{i}{3}(\gamma_M + \gamma_D + \gamma_Q) \tag{6}$$

$$k_x^{\mathrm{EP3}} = \pm\frac{1}{3v_{MD}}\sqrt{\frac{(\gamma_D + \gamma_Q - 2\gamma_M)^3}{3(\gamma_Q - \gamma_M)}} \tag{7}$$

$$k_y^{\mathrm{EP3}} = \pm\frac{1}{3v_{QD}}\sqrt{\frac{(2\gamma_Q - \gamma_M - \gamma_D)^3}{3(\gamma_Q - \gamma_M)}} \tag{8}$$

where, any choice of distinct $\gamma$ leading to real $\mathbf{k}$ induces an EP3. In a lattice with $C_{4v}$ symmetry, this condition cannot be satisfied, unless the symmetry relating the two dipolar modes is severely and intentionally broken. Such a design would necessitate an overlay of spatially varying regions of gain and loss, a scenario that seems experimentally challenging. In contrast, we now present a novel design method that can discover PhC geometries supporting accidental and tunable D3s.

*Inverse-design method.*—We construct an accidental D3 by employing a large-scale optimization strategy that can discover novel topologies and geometries difficult to conceive through conventional intuition. One such strategy, known as topology optimization, employs powerful gradient-based numerical algorithms capable of handling a very large design space, typically considering every pixel or voxel as a degree of freedom (DOF) in an extensive computational domain.

Our approach extends the work of Ref. [38], which showed that it is possible to design a structure supporting a resonant mode at some arbitrary frequency by maximizing the time-averaged power output $f = -\mathrm{Re}[\int \mathbf{J}^* \cdot \mathbf{E} d\mathbf{r}]$ emitted from a time harmonic current source $\mathbf{J}$ at the desired frequency $\omega$, where the electric field response $\mathbf{E}$ is given by the solution of Maxwell's equations, $\nabla \times (1/\mu)\nabla \times \mathbf{E} - \omega^2\epsilon(\mathbf{r})\mathbf{E} = i\omega\mathbf{J}$ [38]. To ensure that the designed resonance has the requisite modal profile, the current $\mathbf{J}$ must be judiciously constructed. For example, to design a transverse magnetic (TM) polarized monopolar mode at the $\Gamma$ point of a PhC, $\mathbf{J}$ should can be chosen as a point dipole $\mathbf{J} = \delta(\mathbf{r} - \mathbf{r}_0)\mathbf{e}_z$ at the center $\mathbf{r}_0$ of the unit cell. Once the objective function $f$ is identified, its gradient with respective to $\epsilon(\mathbf{r})$ can be calculated by the so-called adjoint variable method [37,38] and then supplied to any large-scale gradient-based optimization algorithm such as the method of moving asymptotes (MMAs) [44]. To design structures supporting multiple modes at the same frequency with the requisite ($M$, $D$, $Q$) symmetries, we seek a maxmin formulation in which one maximizes the minimum of $\{f_M, f_D, f_Q\}$, with currents chosen to ensure fields with the desired symmetries, discussed in detail in the Supplemental Material [45].

Our TO framework can be exploited to design high-order degeneracies with distinct modal properties in arbitrary material systems and photonic structures. Here, we use it to demonstrate third-order degeneracies in binary dielectric or air square lattices. Figure 1 (left) shows three such structures, involving materials (in air) of refractive indices $\{2, 3, 1.82\}$ corresponding to (upper, middle, lower) figures with periodicities $a = \{1.05, 0.6, 1\}\lambda$, respectively, where $\lambda$ is the design wavelength in vacuum. Note that such refractive indices are typical for common materials such as silicon nitride, lithium niobate, diamond, silicon, alumina, or ceramics at optical, microwave, and terahertz frequencies. We focus our discussion on the structure with index = 2, leaving details of the two other designs to the Supplemental Material [45]. Noticeably, the band structure of this lattice exhibits a D3 comprising $M$, $D$, and $Q$ modes at the $\Gamma$ point, shown in Fig. 1 (lower right). Note that since the optimized PhC lacks $C_{4v}$ symmetry (but possesses $C_{2v}$), there is only one dipolar mode at the designated frequency and hence, the degeneracy of the three modes is completely

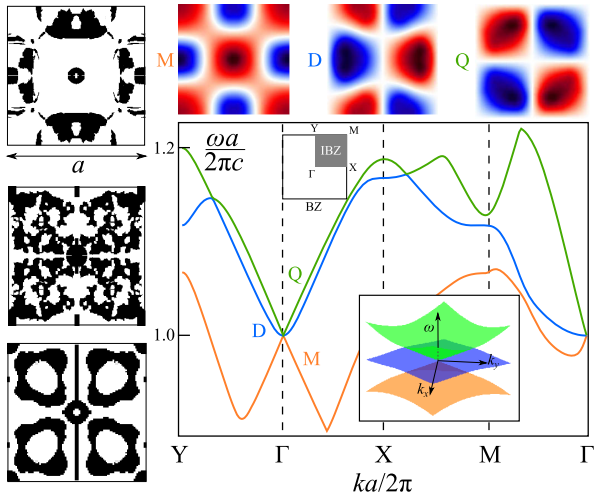


FIG. 1. Inverse-designed 2D square lattices comprising refractive indices $= \{2, 3, 1.82\}$ (upper, middle, and lower schematics) materials in air (white regions), with periodicity $a = \{1.05, 0.6, 1\}\lambda$. Lower right: Band structure of the lattice with refractive index $= 2$ (upper schematic), revealing a Dirac point induced by the presence of an *accidental* third-order degeneracy (D3) of monopolar ($M$), dipolar ($D$), and quadrupolar ($Q$) modes (upper insets). A schematic of the Brillouin zone (BZ) denoting high-symmetry $\mathbf{k}$ points ($Y$, $\Gamma$, $X$, $M$) is also shown. Because of the lack of $C_{4v}$ symmetry, the dispersions along the $X$ and $Y$ directions differ.

*accidental*: potential mode mixing and avoided crossings at the $\Gamma$ point are prevented by the corresponding mirror symmetries. In the vicinity of the trimodal degeneracy, the band structure exhibits conical Dirac dispersion accompanied by a quadratic flat band. While general rules regarding the occurrence of Dirac point dispersion in the vicinity of a modal degeneracy are well understood from group theoretic considerations, e.g., as arising from *two* different irreducible representations [43], to our knowledge our TO-designed PhC is the first demonstration of a Dirac point formed by *three* degenerate modes belonging to *three* different representations, namely, the $A_1$, $A_2$, and $B_1$ representations of the $C_{2v}$ group.

*Third-order exceptional point.*—The third order Dirac degeneracy of Fig. 1 can be straightforwardly linked to an EP3 through the introduction of non-Hermiticity, i.e., material loss, gain, or open boundaries (radiation). Here, we consider such an EP3 by introducing a small imaginary part in the dielectric constant, $\kappa = \sqrt{\mathrm{Im}[\epsilon]} = 0.005$, representing intrinsic material loss and resulting in small decay rates $\{\gamma_M, \gamma_D, \gamma_Q\}/\omega_0 \approx \{3.6, 4.3, 4.2\} \times 10^{-4}$. From Eqs. (7), (8), it follows that there exists an EP3 at $\mathrm{Re}[\omega_{\mathrm{EP3}}] \approx \omega_0$, $\mathrm{Im}[\omega_{\mathrm{EP3}}] \approx 4 \times 10^{-4}(2\pi c/a)$, $k_x^{\mathrm{EP3}} \approx 7 \times 10^{-5}(2\pi/a)$ and $k_y^{\mathrm{EP3}} \approx 1.8 \times 10^{-5}(2\pi/a)$ [45]. Figures 2(a) and 2(c) show the band structure in the vicinity of the $\Gamma$ point, along with slices, Figs. 2(b) and 2(d), indicated by red arrows, illustrating the coalescence of both the real and imaginary mode frequencies. Yet another interesting feature of the dispersion landscape is that, apart from the EP3, there also exists a contour of EP2 (blue lines), defined by $P(\omega; k_x, k_y) = 0$, $P'(\omega; k_x, k_y) = 0$, similar to the ring of EP2 observed in Ref. [8].

A defining signature of non-Hermitian systems is that eigenvectors are no longer orthogonal. Rather, they are bi-orthogonal [10] in the sense of an unconjugated "inner product" between left and right eigenvectors, $(\Psi_n^L)^T \Psi_m^R = \delta_{nm}$, defined such that $A\Psi^R = \omega^2 \Psi^R$ and $A^T \Psi^L = \omega^2 \Psi^L$, where $A$ is the Maxwell operator $\hat{\epsilon}^{-1}(\nabla + i\mathbf{k}) \times (1/\mu)(\nabla + i\mathbf{k})\times$ under Bloch boundary conditions at a specific $\mathbf{k}$, $\hat{\epsilon}$ is the diagonal permittivity tensor $\epsilon(\mathbf{r})$. At our EP3, the three eigenmodes coalesce and become self-orthogonal [16], leading to vanishing inner products

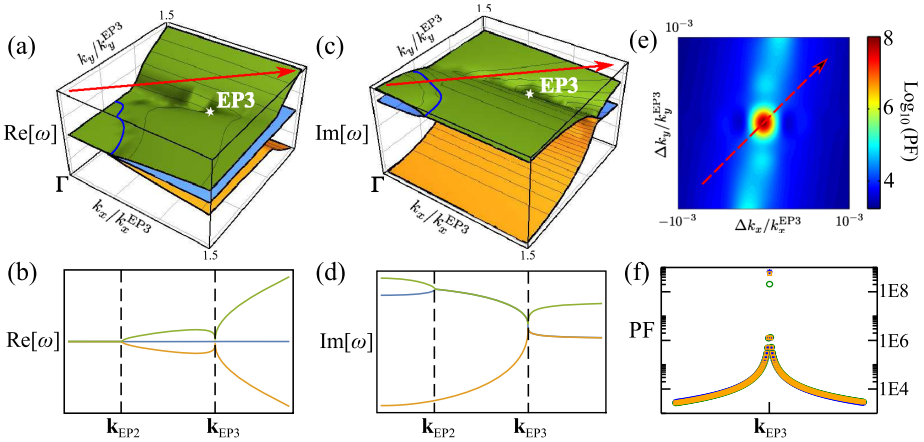


FIG. 2. (a) Real and (c) imaginary eigenfrequencies as a function of $k_x$ and $k_y$ in the vicinity of a third order exceptional point (EP3) of the structure described in Fig. 1, located at $\mathbf{k}^{\mathrm{EP3}} \approx \{7, 1.8\} \times 10^{-5}(2\pi/a)$ (red dot). The blue contours denote regions of second-order exceptional points where two of the three modes coalesce. The plots in (b) and (d) show the corresponding band structures along the $\mathbf{k}$ lines marked by red arrows. (e) Contour plot showing the enhanced Petermann factor (PF) associated with one of the modes in the vicinity of the EP3, and (f) corresponding enhancement along the direction shown by the red arrow, for all three modes.

$(\Psi_n^L)^T\Psi_n^R = 0, n \in \{1,2,3\}$, as characterized by the so-called Petermann factor (PF),

$$\mathrm{PF}_n = \frac{||\Psi_n^L||^2||\Psi_n^R||^2}{|(\Psi_n^L)^T\Psi_n^R|^2} \tag{9}$$

where $||\cdots||^2$ is the usual $L_2$ norm given by $||\Psi||^2 = \Psi^{T*}\Psi$. Figures 2(e) and 2(f) illustrate the divergence of the PF for all three modes as $\mathbf{k} \to \mathbf{k}^{\mathrm{EP3}}$. Note that there are also PF divergences associated with the $M$, $D$ modes at the EP2 contours.

*Local density of states.*—The divergence of the Petermann factor in open systems can lead to many important effects [11,51]. In particular, the SE rate of emitters in resonant cavities is traditionally expressed via the PF (a generalization of the Purcell factor [51]), becoming most pronounced near EPs where the latter diverges [52]. More rigorously, however, the SE rate is given by the LDOS, or the electromagnetic Green's function (GF), which, though enhanced, turns out to be finite even at EPs [22]: coalescent eigenmodes no longer form a complete basis, requiring instead an augmented basis of associated Jordan modes and hence a different definition of LDOS. Such an expansion was recently employed in Ref. [22] to demonstrate limits to LDOS at EP2s in both passive and active media; here, we extend these results to the case of EP3s.

The LDOS at an EP3 can be obtained from the diagonal elements of the imaginary part of the dyadic GF [45]:

$$\mathbb{G}_{\mathrm{EP3}} \approx \frac{\Psi_{\mathrm{EP3}}^R(\Psi_{\mathrm{EP3}}^L)^T}{(\omega^2-\omega_{\mathrm{EP3}}^2)^3} + \frac{\Psi_{\mathrm{EP3}}^R(\Phi_{\mathrm{I}}^L)^T + \Phi_{\mathrm{I}}^R(\Psi_{\mathrm{EP3}}^L)^T}{(\omega^2-\omega_{\mathrm{EP3}}^2)^2} + \frac{\Psi_{\mathrm{EP3}}^R(\Phi_{\mathrm{II}}^L)^T + \Phi_{\mathrm{I}}^R(\Phi_{\mathrm{I}}^L)^T + \Phi_{\mathrm{II}}^R(\Psi_{\mathrm{EP3}}^L)^T}{\omega^2-\omega_{\mathrm{EP3}}^2}. \tag{10}$$

Equation (10) involves a complicated sum of cubic, quadratic, and linear Lorentzian profiles weighted by the outer products of the only surviving left (right) eigenmode $\Psi_{\mathrm{EP3}}^{(L,R)}$ and the two associated Jordan vectors $\Phi_{(\mathrm{I,II})}^{(L,R)}$, determined by the third-order Jordan decomposition of the Maxwell eigenproblem,

$$A_{\mathrm{EP3}}\Psi_{\mathrm{EP3}}^R = \omega_{\mathrm{EP3}}^2\Psi_{\mathrm{EP3}}^R \tag{11}$$

$$A_{\mathrm{EP3}}\Phi_{\mathrm{I}}^R = \omega_{\mathrm{EP3}}^2\Phi_{\mathrm{I}}^R + \Psi_{\mathrm{EP3}}^R \tag{12}$$

$$A_{\mathrm{EP3}}\Phi_{\mathrm{II}}^R = \omega_{\mathrm{EP3}}^2\Phi_{\mathrm{II}}^R + \Phi_{\mathrm{I}}^R, \tag{13}$$

and its associated dual. Equation (10) reveals that the LDOS spectrum $\sim -\mathrm{Im}[\mathrm{Tr}(\mathbb{G})]$ can vary dramatically depending on position, frequency, and decay rates.

Figure 3(a) shows the LDOS spectra at the center of the unit cell $\mathbf{r}_0$, evaluated at either $\mathbf{k}^{\mathrm{EP3}}$ (red curves) or a point $\mathbf{k} = \{7, 1.8\} \times 10^{-2}(2\pi/a) \gg \mathbf{k}^{\mathrm{EP3}}$ (blue curves) far away from the EP3, demonstrating an enhancement factor of $\approx$2.33 in this geometry. Figures 3(c)–3(f) show the corresponding spatial LDOS profiles at and off the EP3, illustrating the seamless coalescence of the eigenmodes. Even greater enhancements are possible under different loss profiles, i.e., $\gamma_M$, $\gamma_D$ and $\gamma_Q$, as illustrated by the following analysis based on the reduced Hamiltonian framework above. In particular, the GF at a given location in the unit cell can be directly related to the diagonal entries of the resolvent of $\mathcal{H}$, defined as $G \equiv (\mathcal{H} - \omega\mathbb{I})^{-1}$. For example, the third entry of $G$ yields the LDOS at points where the intensity of the quadrupole mode dominates. Consider a scenario in which only the monopole mode has a finite lifetime, i.e., $\gamma_M = \gamma$ while $\gamma_D = \gamma_Q = 0$. It follows from Eq. (2) and Eq. (10) that the LDOS in this case is given by,

$$\begin{aligned} &-\mathrm{Im}\{G_{\mathrm{EP3}}[3,3]\} \\ &\approx -\frac{2\gamma^2}{27}\frac{\bar{\gamma}^3 - 3\bar{\gamma}(\mathrm{Re}[\omega_{\mathrm{EP3}}]-\omega)^2}{(\mathrm{Re}[\omega_{\mathrm{EP3}}]-\omega)^2+\bar{\gamma}^2]^3} \\ &\quad + \frac{\gamma}{3}\frac{\bar{\gamma}^2 - (\mathrm{Re}[\omega_{\mathrm{EP3}}]-\omega)^2}{[(\mathrm{Re}[\omega_{\mathrm{EP3}}]-\omega)^2+\bar{\gamma}^2]^2} - \frac{\bar{\gamma}}{(\mathrm{Re}[\omega_{\mathrm{EP3}}]-\omega)^2+\bar{\gamma}^2}, \end{aligned} \tag{14}$$

where $\bar{\gamma} \equiv \gamma/3$. Moreover, the peak LDOS at $\omega = \mathrm{Re}[\omega_{\mathrm{EP3}}]$ is found to be $8/\gamma$, corresponding to an eightfold enhancement relative to the peak LDOS far away from the EP3. Such an enhancement is illustrated in Fig. 3(b), which also reveals the highly non-Lorentzian spectrum associated with this EP3. We remark that this enhancement in LDOS does

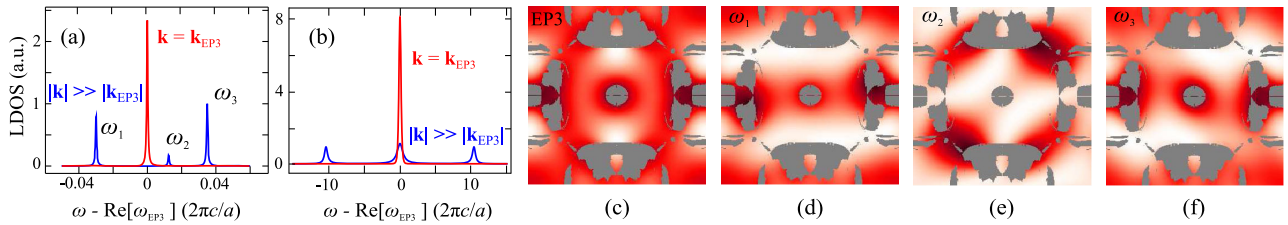


FIG. 3. (a) Local density of states (LDOS) at the center of the unit cell of the structure in Fig. 1, evaluated at either $\mathbf{k}^{\mathrm{EP3}} \approx \{7, 1.8\} \times 10^{-5}(2\pi/a)$ (red curves) or $\mathbf{k} = \{7, 1.8\} \times 10^{-2}(2\pi/a) \gg \mathbf{k}^{\mathrm{EP3}}$ (blue curves). (b) Maximum (eightfold) LDOS enhancement associated with an EP3, computed via the reduced $3 \times 3$ Hamiltonian model of (2). (c)–(f) LDOS profiles evaluated at either $\omega_{\mathrm{EP3}}$ or at the nondegenerate frequencies $\omega_1$, $\omega_2$, and $\omega_3$, corresponding to the EP3 and far-away points described in (a). Note that the LDOS is evaluated only in air regions since the LDOS within a lossy medium formally diverges [53].

not lead to additional dissipation, which is made clear upon observing that the loss rates (described by the imaginary parts of the complex eigenfrequencies) remain roughly the same at and away from the EP. Instead, it arises from the complex, constructive interference of these modes, as mediated by the decay channels. Note also that similar enhancements can also be realized in nondissipative media so long as there exist decay channels leading to non-Hermiticity (e.g., radiative or coupling losses).

It is possible to exploit a simple sum rule, namely, that the spectrally integrated LDOS is a constant [54], to predict the maximum enhancement possible for an EP of arbitrary order $n$. In particular, the integrated LDOS of an order-$n$ Lorentzian of the form $L_n(\omega) = (\gamma^{2n-1}c_n/[(\omega - \mathrm{Re}[\omega_{\mathrm{EP}n}])^2 + \gamma^2]^n)$ is $S_n(\omega) = \int d\omega L_n(\omega) = (c_n\sqrt{\pi}\Gamma[n-\frac{1}{2}]/\Gamma[n])$, where $\Gamma$ is the gamma function. It follows from the sum rule that $nS_1(\omega) = S_n(\omega)$ and, consequently, that $c_n/c_1 = (\sqrt{\pi}\Gamma[n+1]/\Gamma[n-\frac{1}{2}]) \sim \sqrt{n^3}$ for large $n \gg 1$. In the case of an EP3, the maximum enhancement $c_3/c_1 = 8$, which is realized in the scenario discussed above.

*Concluding remarks.*—Although fabrication of the above "bar-code" structures may prove challenging at visible wavelengths using currently available technologies, future experimental realizations are entirely feasible in the midinfrared to microwave regimes, where complex features can be straightforwardly fabricated in polymers and ceramics with the aid of computerized machining, 3D printing, laser cutting, additive manufacturing, or two-photon lithography [55–57]. In particular, the low-index (refractive index = 1.82) design (Fig. 1 lower schematic) exhibits regular and relatively smooth features (the smallest of which ~150 nm for operation at mid-IR wavelengths), making it accessible to standard electron-beam lithography techniques. Furthermore, while the above predictions offer a proof of principle, the same inverse-design techniques can be applied to the design of higher-order EPs as well as other topologies, including cavities. Our ongoing work in this regard includes the design of chiral modes, photonic Weyl points, topological insulators, and omnidirectional Dirac-cone, zero-index metamaterials.

We would like to thank Steven G. Johnson for useful discussions. This work was partially supported by the Air Force Office of Scientific Research under Contract No. FA9550-14-1-0389, by the National Science Foundation under Grant No. DMR-1454836, and by the Princeton Center for Complex Materials, a MRSEC supported by NSF Grant No. DMR 1420541. Z. Lin is supported by the National Science Foundation Graduate Research Fellowship Program under Grant No. DGE1144152.

*zinlin@g.harvard.edu

[1] S.-L. Chua, L. Lu, J. Bravo-Abad, J. D. Joannopoulos, and M. Soljačić, Larger-area single-mode photonic crystal surface-emitting lasers enabled by an accidental dirac point, Opt. Lett. **39**, 2072 (2014).

[2] X. Zhang, Observing Zitterbewegung for Photons near the Dirac Point of a Two-Dimensional Photonic Crystal, Phys. Rev. Lett. **100**, 113903 (2008).

[3] X. Huang, Y. Lai, Z. H. Hang, H. Zheng, and C. T. Chan, Dirac cones induced by accidental degeneracy in photonic crystals and zero-refractive-index materials, Nat. Mater. **10**, 582 (2011).

[4] Y. Li, S. Kita, P. Muñoz, O. Reshef, D. I. Vulis, M. Yin, M. Lončar, and E. Mazur, On-chip zero-index metamaterials, Nat. Photonics **9**, 738 (2015).

[5] S. Raghu and F. D. M. Haldane, Analogs of quantum-hall-effect edge states in photonic crystals, Phys. Rev. A **78**, 033834 (2008).

[6] A. B. Khanikaev, S. Hossein Mousavi, W.-K. Tse, M. Kargarian, A. H. MacDonald, and G. Shvets, Photonic topological insulators, Nat. Mater.. **12**, 233 (2013).

[7] L. Lu, C. Fang, L. Fu, S. G. Johnson, J. D. Joannopoulos, and M. Soljacic, Symmetry-protected topological photonic crystal in three dimensions, Nat. Phys. **12**, 337 (2016).

[8] B. Zhen, C. W. Hsu, Y. Igarashi, L. Lu, I. Kaminer, A. Pick, S.-L. Chua, J. D. Joannopoulos, and M. Soljacic, Spawning rings of exceptional points out of dirac cones, Nature (London) **525**, 354 (2015).

[9] N. Moiseyev, *Non-Hermitian Quantum Mechanics* (Cambridge University Press, Cambridge, 2011).

[10] T. Kato, *Perturbation Theory for Linear Operators* (Springer-Verlag, Berlin, 1995).

[11] M. V. Berry, Physics of non-Hermitian degeneracies, Czech. J. Phys. **54**, 1039 (2004).

[12] W. D. Heiss, The physics of exceptional points, J. Phys. A **45**, 444016 (2012).

[13] C. M. Bender and S. Boettcher, Real Spectra in Non-Hermitian Hamiltonians Having $\mathcal{PT}$ Symmetry, Phys. Rev. Lett. **80**, 5243 (1998).

[14] C. E. Ruter, K. G. Makris, R. El-Ganainy, D. N. Christodoulides, M. Segev, and D. Kip, Observation of parity-time symmetry in optics, Nat. Phys. **6**, 192 (2010).

[15] A. Guo, G. J. Salamo, D. Duchesne, R. Morandotti, M. Volatier-Ravat, V. Aimez, G. A. Siviloglou, and D. N. Christodoulides, Observation of $\mathcal{PT}$-Symmetry Breaking in Complex Optical Potentials, Phys. Rev. Lett. **103**, 093902 (2009).

[16] M. C. Zheng, D. N. Christodoulides, R. Fleischmann, and T. Kottos, Optical lattices and universality in beam dynamics, Phys. Rev. A **82**, 010103 (2010).

[17] H. Ramezani, T. Kottos, V. Kovanis, and D. N. Christodoulides, Exceptional-point dynamics in photonic honeycomb lattices with symmetry, Phys. Rev. A **85**, 013818 (2012).

[18] S. Longhi and G. D. Valle, Optical lattices with exceptional points in the continuum, Phys. Rev. A **89**, 052132 (2014).

[19] L. Ge and A. Douglas Stone, Parity-Time Symmetry Breaking beyond One Dimension: The Role of Degeneracy, Phys. Rev. X **4**, 031011 (2014).

[20] A. Cerjan, A. Raman, and S. Fan, Exceptional Contours and Band Structure Design in Parity-Time Symmetric Photonic Crystals, Phys. Rev. Lett. **116**, 203902 (2016).

[21] M. V. Berry, Mode degeneracies and the petermann excess-noise factor for unstable lasers, J. Mod. Opt. **50**, 63 (2003).

[22] A. Pick, B. Zhen, O. D. Miller, C. W. Hsu, F. Hernandez, A. W. Rodriguez, M. Soljačić, and S. G. Johnson, General theory of spontaneous emission near exceptional points, arXiv:1604.06478.

[23] C. Dembowski, B. Dietz, H.-D. Gräf, H. L. Harney, A. Heine, W. D. Heiss, and A. Richter, Observation of a Chiral State in a Microwave Cavity, Phys. Rev. Lett. **90**, 034101 (2003).

[24] Z. Lin, H. Ramezani, T. Eichelkraut, T. Kottos, H. Cao, and D. N. Christodoulides, Unidirectional Invisibility Induced by $\mathcal{PT}$-Symmetric Periodic Structures, Phys. Rev. Lett. **106**, 213901 (2011).

[25] L. Feng, Y.-L. Xu, W. S. Fegadolli, M.-H. Lu, J. B. Oliveira, V. R. Almeida, Y.-F. Chen, and A. Scherer, Experimental demonstration of a unidirectional reflectionless parity-time metamaterial at optical frequencies, Nat. Mater. **12**, 108 (2013).

[26] M. Liertzer, L. Ge, A. Cerjan, A. D. Stone, H. E. Türeci, and S. Rotter, Pump-Induced Exceptional Points in Lasers, Phys. Rev. Lett. **108**, 173901 (2012).

[27] H. Hodaei, M.-A. Miri, M. Heinrich, D. N. Christodoulides, and M. Khajavikhan, Parity-time–symmetric microring lasers, Science **346**, 975 (2014).

[28] L. Feng, Z. J. Wong, R.-M. Ma, Y. Wang, and X. Zhang, Single-mode laser by parity-time symmetry breaking, Science **346**, 972 (2014).

[29] T. Gao, E. Estrecho, K. Y. Bliokh, T. C. H. Liew, M. D. Fraser, S. Brodbeck, M. Kamp, C. Schneider, S. Hofling, Y. Yamamoto, F. Nori, Y. S. Kivshar, A. G. Truscott, R. G. Dall, and E. A. Ostrovskaya, Observation of non-Hermitian degeneracies in a chaotic exciton-polariton billiard, Nature (London) **526**, 554 (2015).

[30] E. M. Graefe, U. Günther, H. J. Korsch, and A. E. Niederle, A non-Hermitian $\mathcal{PT}$ symmetric Bose-Hubbard model: Eigenvalue rings from unfolding higher-order exceptional points, J. Phys. A **41**, 255206 (2008).

[31] J.-W. Ryu, S.-Y. Lee, and S. W. Kim, Analysis of multiple exceptional points related to three interacting eigenmodes in a non-Hermitian hamiltonian, Phys. Rev. A **85**, 042101 (2012).

[32] W. D. Heiss and G. Wunner, Resonance scattering at third-order exceptional points, J. Phys. A **48**, 345203 (2015).

[33] K. Ding, G. Ma, M. Xiao, Z. Q. Zhang, and C. T. Chan, Emergence, Coalescence, and Topological Properties of Multiple Exceptional Points and their Experimental Realization, Phys. Rev. X **6**, 021007 (2016).

[34] By accidental degeneracy, we mean that the frequency collision is neither induced nor protected by any underlying point symmetry, but rather is entirely fashioned out of the detailed morphology of the photonic unit cell, designed via brute-force topology optimization techniques.

[35] O. Sigmund and J. S. Jensen, Systematic design of phononic band–gap materials and structures by topology optimization, Phil. Trans. R. Soc. A **361**, 1001 (2003).

[36] M. Burger, S. J. Osher, and E. Yablonovitch, Inverse problem techniques for the design of photonic crystals, IEICE Trans. Electron. **87**, 258 (2004).

[37] J. S. Jensen and O. Sigmund, Topology optimization for nano-photonics, Laser Photonics Rev. **5**, 308 (2011).

[38] X. Liang and S. G. Johnson, Formulation for scalable optimization of microcavities via the frequency-averaged local density of states, Opt. Express **21**, 30812 (2013).

[39] A. Y. Piggott, J. Lu, K. G. Lagoudakis, J. Petykiewicz, T. M. Babinec, and J. Vuckovic, Inverse design and demonstration of a compact and broadband on-chip wavelength demultiplexer, Nat. Photonics **9**, 374 (2015).

[40] B. Shen, P. Wang, and R. Menon, An integrated-nanophotonics polarization beamsplitter with $2.4 \times 2.4$ um$^2$ footprint, Nat. Photonics **9**, 378 (2015).

[41] Z. Lin, X. Liang, M. Lončar, S. G. Johnson, and A. W. Rodriguez, Cavity-enhanced second-harmonic generation via nonlinear-overlap optimization, Optica **3**, 233 (2016).

[42] J. Mei, Y. Wu, C. T. Chan, and Z.-Q. Zhang, First-principles study of dirac and dirac-like cones in phononic and photonic crystals, Phys. Rev. B **86**, 035141 (2012).

[43] K. Sakoda, Proof of the universality of mode symmetries in creating photonic dirac cones, Opt. Express **20**, 25181 (2012).

[44] K. Svanberg, A class of globally convergent optimization methods based on conservative convex separable approximations, SIAM J. Optim. **12**, 555 (2002).

[45] See Supplemental Material at http://link.aps.org/supplemental/10.1103/PhysRevLett.117.107402 for detailed methods and derivations, which includes Refs. [46–50].

[46] A. Taflove, A. Oskooi, and S. G. Johnson, *Advances in FDTD Computational Electrodynamics: Photonics and Nanotechnology* (Artech House, Norwood, 2013).

[47] G. B. Arfken and H. J. Weber, *Mathematical Methods for Physicists* (Elsevier Academic Press, New York, 2006).

[48] A. Mailybaev and A. P. Seyranian, On singularities of a boundary of the stability domain, SIAM J. Matrix Anal. Appl. **21**, 106 (1999).

[49] G. Demange and E.-M. Graefe, Signatures of three coalescing eigenfunctions, J. Phys. A **45**, 025303 (2012).

[50] A. P. Seyranian and A. A. Mailybaev, *Multiparameter Stability Theory With Mechanical Applications* (World Scientific Publishing, Singapore, 2003).

[51] K. Petermann, Calculated spontaneous emission factor for double-heterostructure injection lasers with gain-induced waveguiding, IEEE J. Quantum Electron. **15**, 566 (1979).

[52] M. V. Berry, Mode degeneracies and the petermann excess-noise factor for unstable lasers, J. Mod. Opt. **50**, 63 (2003).

[53] S. Scheel, L. Knöll, and D.-G. Welsch, Spontaneous decay of an excited atom in an absorbing dielectric, Phys. Rev. A **60**, 4094 (1999).

[54] S. M. Barnett and R. Loudon, Sum Rule for Modified Spontaneous Emission Rates, Phys. Rev. Lett. **77**, 2444 (1996).

[55] R. A. Borisov, G. N. Dorojkina, N. I. Koroteev, V. M. Kozenkov, S. A. Magnitskii, D. V. Malakhov, A. V. Tarasishin, and A. M. Zheltikov, Fabrication of three-dimensional periodic microstructures by means of two-photon polymerization, Appl. Phys. B **67**, 765 (1998).

[56] A. Clausen, F. Wang, J. S. Jensen, O. Sigmund, and J. A. Lewis, Topology optimized architectures with programmable Poisson's ratio over large deformations, Adv. Mater. **27**, 5523 (2015).

[57] C. Pouya, J. T. B. Overvelde, M. Kolle, J. Aizenberg, K. Bertoldi, J. C. Weaver, and P. Vukusic, Characterization of a mechanically tunable gyroid photonic crystal inspired by the butterfly parides sesostris, Adv. Opt. Mater. **4**, 99 (2016).